4th International Conference on Recent Development in Engineering Science, Humanities and Management
National Institute of Technical Teachers Training & Research, Chandigarh, India (ESHM-17)
2nd April 2017, www.conferenceworld.in ISBN: 978-93-86171-19-1

Synthesis and Characterizations of Europium doped Silica Nanophosphor

Rachna Ahlawat

Assistant Professor, Department of Physics,
Ch. Devi Lal University, Sirsa, Haryana (India)

ABSTRACT

Rare earth activated oxide Nanophosphors were produced by drying the precursor gels at room temperature followed by annealing at 500^oC and 1000^oC in ambient air. The phase and morphology of the nanopowder was determined by X-ray diffraction, FTIR and TEM. The crystallite size was estimated with the Scherrer formula and found ~ 30 nm. The change in luminescence properties in transforming from amorphous to monoclinic phase due to temperature effect are discussed at length. Here red shift has occurred in optical absorption spectra for all prepared samples with temperature. Band gap energy was also calculated using well known Tauc's plot. This mechanism revealed that Eu^{3+} ions incorporated into a SiO_2 matrix by a sol–gel process is significantly affected by annealing temperature and resulting in a phosphor that may be used in many applications such as fluorescent lamps, solid state lasers, optical waveguides and field emission display devices.

Keywords: Eu^{3+}:SiO_2, nanophosphors, X-ray diffraction, FTIR, TEM, Uv- Vis.

I. INTRODUCTION

From literature study, it is also known that the rare-earth sesquioxide exist in three different structure types depending upon the ionic radii of the rare earth. The intermediate groups form a monoclinic structure generally belongs to sesquioxide of Pm^{3+}, Sm^{3+}, Eu^{3+}, and Gd^{3+}. Although cubic structure is most stable state for these oxides, they can be transformed to monoclinic modifications after annealing at higher temperature, which can be retained at ambient temperature [1-3]. New fields of applications e.g., novel laser materials, luminescent markers in biological devices, or light-emitting diodes, have been established for such lanthanides based oxide phosphors and there still has been a lot of effort devoted to the further development of new lanthanide-doped materials with improved chemical stability. In this regard, the lanthanide ions must be inserted into a stable inorganic, organic, or inorganic-organic hybrid matrix [4-6]. Particularly, the incorporation of lanthanide ions into inorganic mesoporous hosts with high specific surface areas has attracted much interest in recent years. Silica (SiO_2) is an excellent host material for rare earth ions because of its high transparency, compositional variety and easy mass production. The traditional and most widely used method for producing commercial phosphors- solid state reaction (SSR) always leads to irregular morphologies and wide size distribution [7]. Phosphors produced by SSR may also experience contamination from ball-milling and insufficient dopant mixing. In contrast to this, wet-chemical process are widely accepted in which sol-gel method has many inherent advantages like simple experimental procedure, relatively low reaction temperature, short reaction time with low cost. Powders obtained by this method also have fine grain, narrow size distribution and homogeneous doping of europium ion in silica matrix. Therefore, in the present study synthesis, structural and optical characterizations of Eu^{3+} doped SiO_2 nanophosphor have been carried out by sol-gel technique.

ISBN: 978-93-86171-19-1

II. EXPERIMENTAL

2.1 Sample preparation

The detail mechanism of sample preparation using sol-gel has been demonstrated in the Fig. 2.1.

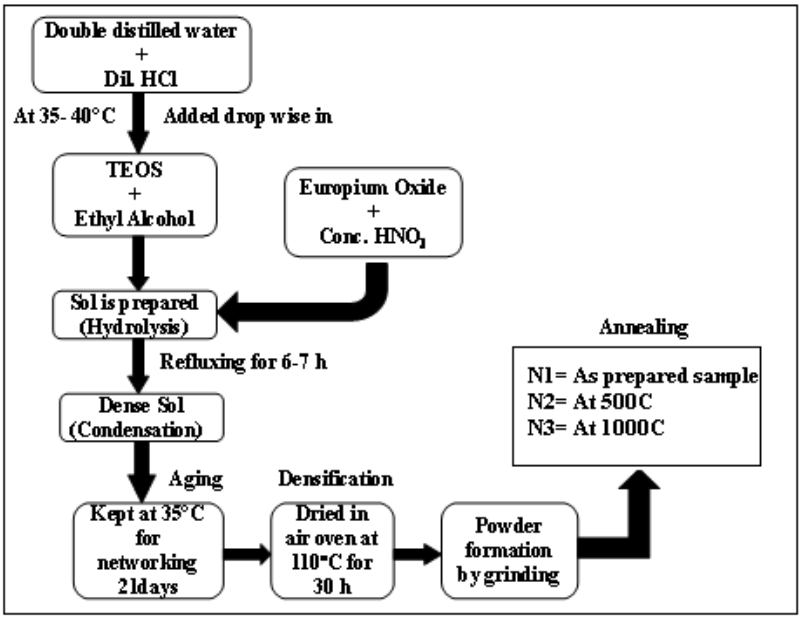

Figure 2.1: Block diagram of sample preparation using sol-gel process.

2.2 Characterizations

All the prepared samples were characterized by well-known techniques like XRD, FTIR, TEM and Uv-Vis spectroscopy. The x-ray diffractograms were taken with the help of XPERT-PRO x-ray diffractometer operated at 45 kV and 40 mA, using monochromatic Cu Kα radiation of wavelength 1.5406 Å in the different 2^{o} ranges. FTIR spectra of the nanocomposites (as-prepared and annealed samples) were taken at room temperature using perkin Elmer 400 spectrophotometer in the range 400-4000 cm^{-1}. The morphology of various samples was confirmed by Hitachi 4500 Transmission Electron Microscope. The optical absorption spectra have been observed by using Lambda 750 (Perkin Elmer) UV-Vis-NIR spectrophotometer in 200-900 nm range.

III. RESULTS AND DISCUSSIONS

3.1 X-Ray Diffraction (XRD) Analysis:

XRD characterization can be used for phase identification, structural analysis and grain size determination of samples N1, N2 and N3. XRD pattern of as prepared sample N1 as shown in Fig. 3.1 has no diffraction peaks due to amorphous nature (JCPDS card no. 29-0085) of silica powder.

ISBN: 978-93-86171-19-1

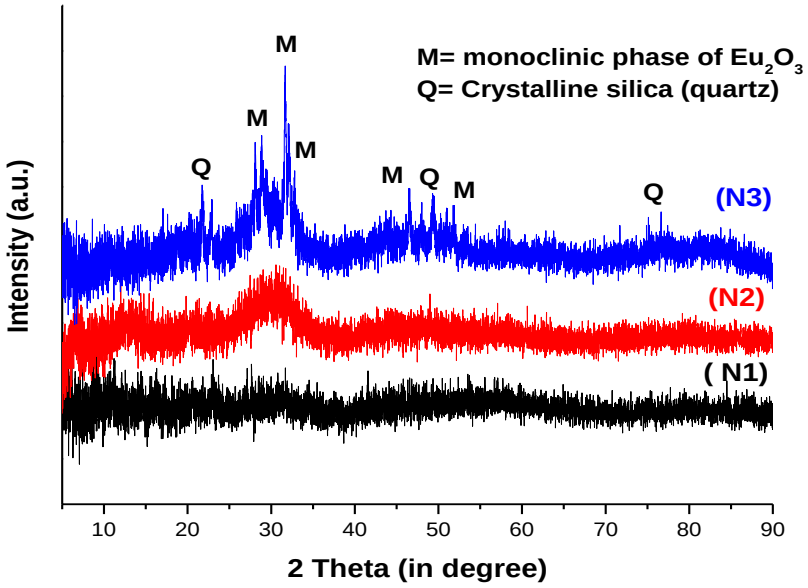

Figure 3.1: XRD pattern of samples N, N2 and N3.

This pattern of dried sample signifies bulk behavior of hydrous precursor's and also suggests that the precursors have not decomposed yet. In general, synthesis at room temperature decomposes the precursor, initiates interfacial reaction between solids and eliminates impurities/pores associated with grain growth. During the synthesis of nanopowder we got different type of structure at different annealing temperatures. Therefore, the samples were annealed at much higher temperature to see the effect of heating. The annealing temperature is selected as 500^{o}C and 1000^{o}C, because at higher temperature T >1000°C, agglomeration of particles increases and conversion of oxides in rare earth silicates starts to form which may alter the luminescent properties.

Fig. 3.1 shows the XRD pattern for sample N2 which is annealed at 500^{o}C. It is emphasized that the XRD pattern has an only broad single peak at 2θ~30^{o}. This feature resembles with the amorphous nature of silica in which a hump is always observed at 2θ~22^{o} [9]. No sharp peak appeared in the XRD pattern of sample N2 which shows completely the amorphous nature of the sample after annealing and also confirms that Eu^{3+} ion is successfully doped into the SiO_2 matrix. This result suggests that the heating of Eu^{3+} doped silica much below its melting temperature is not sufficient (T_m~ 2500^{o}C) for achieving initial crystalline phase of the composite. Some interesting results have been obtained when the sample N3 annealed at much higher temperature (~ 1000^{o}C) as shown in Fig. 3.1. It is observed that the transformation of broad SiO_2 hump into sharper peaks has been occurred in x-ray diffractogram which confirms the crystalline nature of prepared powder. The XRD pattern of this sample revealed that sudden heating at much higher temperature (almost double to sample N2) produces mixed crystalline phases of Eu_2O_3 and crystalline silica (quartz).

3.1.1 Phase Analysis: The X-ray diffraction can be pictured as a reflection of the incident beam from the lattice planes. The Bragg's law ($2d_{hkl}\ Sin\theta_{hkl} = n\lambda$) relates the direction of propagation of scattered beams (θ_{hkl}) to the inter planer distance (d_{nkl}) in the lattice. The crystalline phase for sample N3 calculated from the observed X-ray diffractograms using the check cell programme and JCPDS (Joint Committee Pattern Diffraction Studies) data. In order to identify structure of the polycrystalline phase, plane corresponding to all major diffraction peaks at

 ISBN: 978-93-86171-19-1

2θ ~ 28.94°, 31.64°, 32.12° and 49.35°which are assigned to monoclinic phase of Eu_2O_3 by comparing the obtained data with the JCPDS card no. 34-0072 and space group C2/m. While some minor peaks at 2θ ~ 21.74°, 46.48° and 76.21° could be attributed to the crystalline silica having JCPDS Card No.- 07-0346) [10]. The peaks of monoclinic phase of europium oxide and quartz are represented by letter 'M' and 'Q', respectively as shown in the x-ray diffractogram in the Fig. 3.1.

3.1.2 Identification of Miller Indices: The observed planes have been analyzed using a set of (h,k,l) indices. The 'hkl' index is the property of a material and is related with the lattice constant. In order to identify structure of the polycrystalline phase occurred in N3 sample, plane corresponding to diffraction peaks at 2θ ~ 28.94°, 31.64°, 32.12°, 49.35°could be assigned to Miller indices [111], [310], [112], [512] respectively which are well matched with the other studies [9-10].

3.1.3 Nanocrystalline size calculation: We have calculated average crystalline size for sample N3 using well known Debye-Scherer's equation (1) which is given below:

$$D=K\lambda/\beta\text{Cos}(\theta) \quad (1)$$

Here θ is the Bragg angle of diffraction lines, λ is the wavelength of incident X-ray and β is the full width at half maximum (FWHM). The average size has been calculated as ~30 nm for sample N3. According to Scherrer formula, the peak will be narrow and sharp when the crystal size is bigger. Thus this result can be attributed to the growth of the crystal with annealing temperature.

3.1.4 Estimation of Strain: The micro-strain and crystallite size produces peak broadening in the x-ray diffractogram. The strain effect can be understood by Williamson-Hall plot for sample N3 annealed at 1000°C. The W-H formula is given by following equation (2):

$$\beta_{hkl}\text{Cos}(\theta)_{hkl} = K\lambda/D + 2\varepsilon\,\text{Sin}(\theta)_{hkl} \quad (2)$$

where K is the shape factor which is 0.9 for uniform small size crystals, λ is the wavelength of X-ray, θ_{hkl} is the Bragg angle, ε is the micro-strain and D is an average crystallite size measured in a direction perpendicular to the surface of the specimen. A graph is plotted between 4 Sin $(\theta)_{hkl}$ and β_{hkl} Cos$(\theta)_{hkl}$ as shown in the Fig. 3.2.

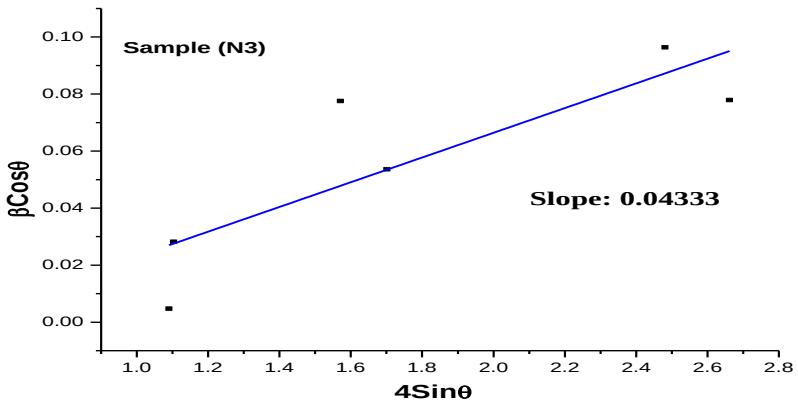

Figure 3.2: W-H Plot for sample N3.

The value of micro-strain is estimated from slope ($\varepsilon = 4.3\times10^{-2}$) of the line and the crystallite size (D~32 nm) was obtained from the intersection with the vertical axis. The grain size determined from W–H formula (equation 2) is slightly higher than those calculated using Scherrer's formula. The small increase in the values is

ISBN: 978-93-86171-19-1

due to the fact that in the case of Scherrer's formula strain component is assumed to be zero and observed broadening of diffraction peak is considered as a result of reducing grain size only [11]. Under such considerations (ε =0), Williamson-Hall relation reduces to Debye-Scherer's formula given in equation (1).

3.2 Fourier Transform Infrared (FTIR) Spectroscopy:

FTIR spectra of Eu^{3+}:SiO_2 composites for as-prepared and annealed samples have been shown in the Fig. 3.3 at room temperature in the spectral range 400-4000 cm^{-1}. These spectra provide valuable information about the phase composition as well as bonding in the prepared samples. It exhibits different intensive sharp, intermediate and broad infrared absorption bands whose data is furnished in the Table 1.

Table 1: FTIR peak list for all samples of Eu^{3+}: SiO_2 nanopowder.

Vibration frequency cm^{-1}	Present Bands	Sample N1	Sample N2	Sample N3
3500-3350	O-H stretching [10]	3405	3442	3432
3000-2800	C-H Bonding [13]	-----	2971	2927, 2857
2350-2200	C=O [10]	2370	2362	2343
1610-1650	H-O-H bending mode	1641	-------	1641
1334-1470	Organic residue and defects [13]	1334,1384, 1470	-------	-------
1150-900	Si-O-Si asymmetric stretching vibration [11]	1040, 1105	1104,967	1022, 931
800-819	Si-O-Si symmetric stretching vibration [12]	819	804	----
600-500	Metal- Oxygen [11]	---	----	558
460-476	Si-O-Si bending vibration [12]	476	467	-----

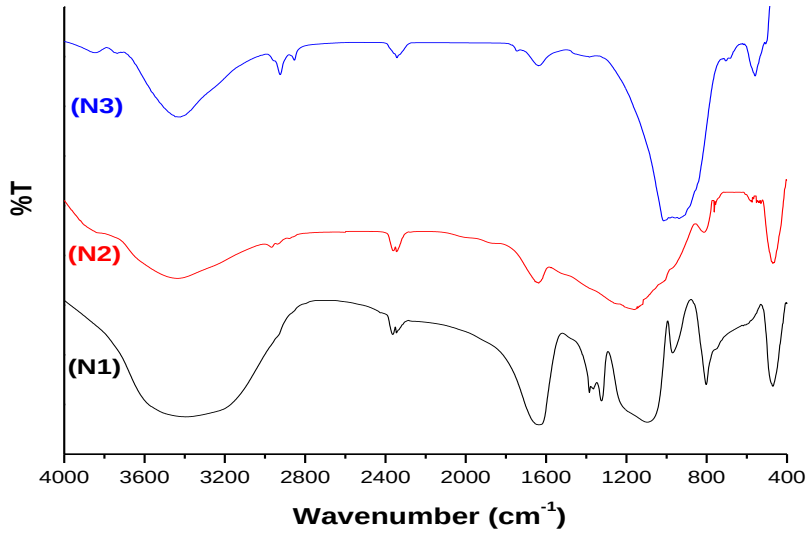

Figure 3.3: FTIR spectrum for sample N1, N2 and N3.

ISBN: 978-93-86171-19-1

3.3 Transmission Electron Microscopy (TEM) Analysis:

The observed TEM micrographs have been shown in the Fig. 3.4 for N1, N2 and N3 samples. TEM was employed to visualize the size and the shape of crystallites and to confirm the nano crystalline nature of the prepared samples. The TEM image of as prepared sample N1 shows some bubbles type structure which indicates the as-formed precursors and confirm the presence of hydroxyl groups in the prepared powder. At this stage the reaction between the precursors i.e. the composite formation is observed between europium hydroxide and the silica networking structure.

One can easily see the trapped water in the micrograph of sample N1. In the micrograph of sample N1 mostly particles are appeared in nanometer scale but appropriate phase was observed due to agglomeration of nanoparticles in amorphous silica [8]. Further, the TEM analysis of sample N2 revealed that the water molecules, hydroxides and nitrides are almost disappeared in the micrograph. However, the densification appeared in the amorphous silica confirms that Eu^{3+} ions are completely implanted at lattice sites. The micrograph of sample N3 exhibits a compact arrangement of almost homogeneously dispersed nanoparticles with almost spherical shape. Fig. 3.4 shows the observed change in structure from amorphous (N1, N2) to monoclinic crystal phase (N3) with average particle size ~30 nm [11]. The SAED pattern for crystalline structure has been shown in the inset of the micrograph for annealed sample N3. The clear rings observed in the SAED pattern of sample N3 verify the better polycrystalline nature than the other two samples. The measured particle size of nanocrystallites is in accordance with calculations from XRD analysis. These luminescent materials are found to be in nano (20-35 nm) range which have applicability in the field of lighting and display technology [14].

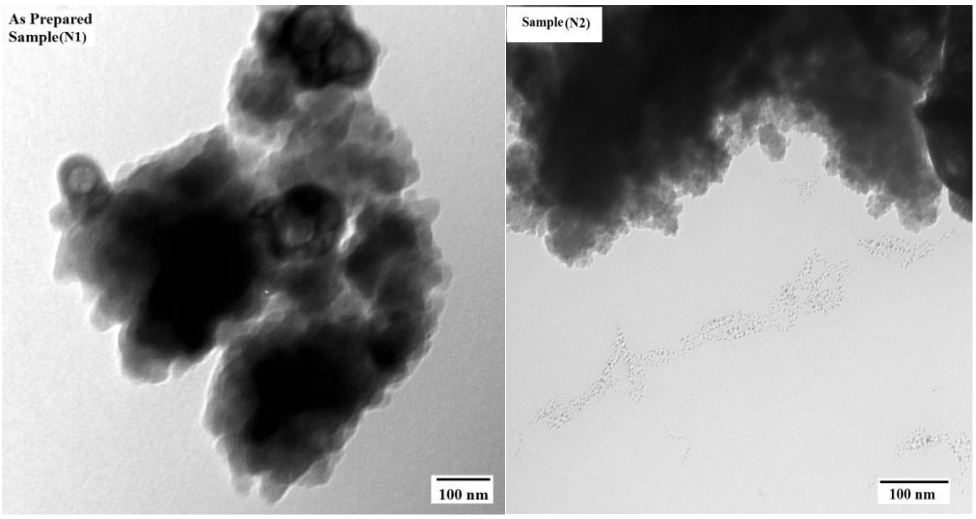

ISBN: 978-93-86171-19-1

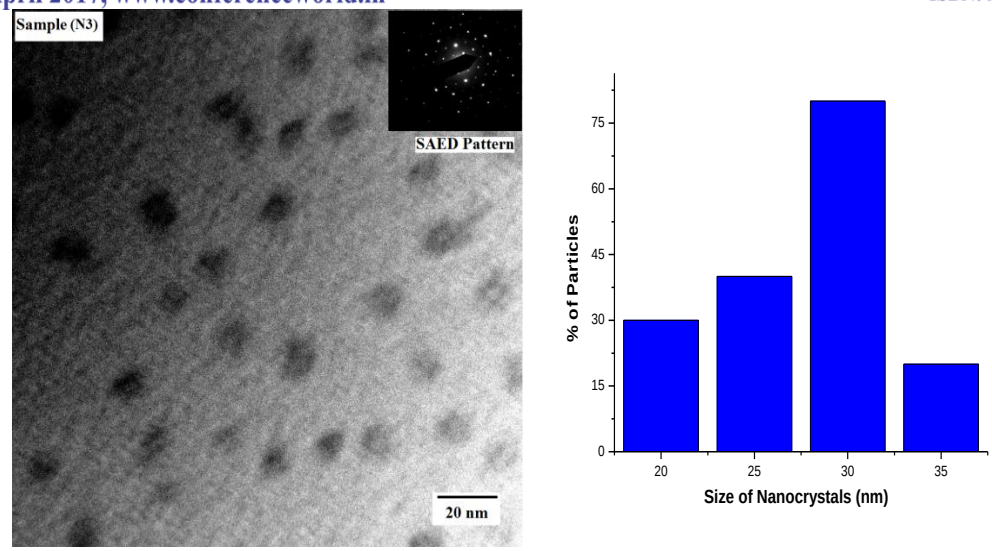

Figure 3.4: TEM image of sample N1, N2, N3 and histogram for annealed sample S3.

3.4 Optical Absorption Spectra:

The UV-Vis absorption spectra of as prepared sample N1 and annealed samples N2, N3 are shown in the Fig. 3.5. The sample N1 has band edge absorption at 307 nm along with two small peaks at 394 and 465 nm. The absorption peak at 305 nm could be attributed from excitation of silica host or may be due to Eu-O charge transfer bond (CTB). It is observed that two small peaks are corresponding to the absorption of Eu^{3+} 4f-4f transitions originated from the ground state $^7F_0$. These small peaks appeared at 394 and 465 nm assigned to the $^7F_0 \longrightarrow {}^5F_6$ and $^7F_0 \longrightarrow {}^5D_2$ transitions, respectively [15].

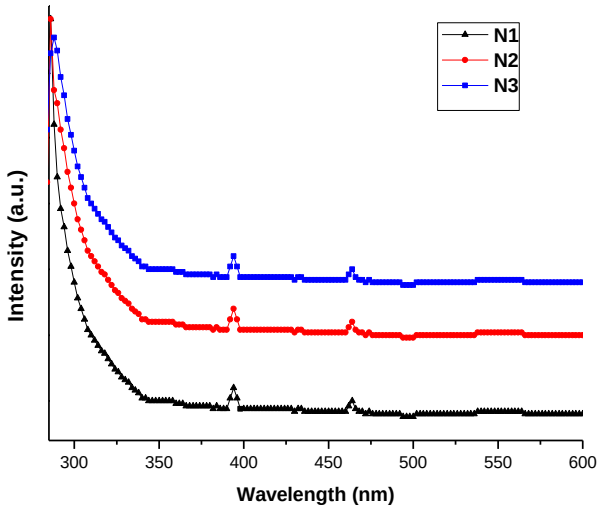

Figure 3.5: Absorption spectra of samples N1, N2 and N3.

The peak intensity corresponding to Eu-O CTB is much higher than that of Eu^{3+} (f-f- absorption) indicating strong energy transfer from Eu-O CTB to Eu^{3+}. The peak intensity of Eu-O CTB increases with increasing of heat treatment temperature up to 1000°C. This is related to extent of reduction of non-radiative process for higher heat treatment samples. In annealed samples, N2 and N3 the band edge absorption peaks shifts towards the higher wavelength side at 320 nm & 330 nm, respectively, which is well matched with literature [16]. The

ISBN: 978-93-86171-19-1

observed shift in the absorption spectra has been occurred due to well-known quantum confinement effect. The relation between the incident photon energy ($h\nu$) and the absorption coefficient (α) is given by the following equation (4):

$$(\alpha h\nu)^{1/n} = A\,(h\nu - E_g) \qquad (4)$$

here A is a constant, α is absorption coefficient and $E_g$is the band gap energy of the material and the exponent *n* depends on the type of transition. For direct allowed transition n = 1/2, for indirect allowed transition n= 2, for direct forbidden n= 3/2 and for indirect forbidden n= 3. Direct band gap of the samples are calculated by plotting $(\alpha h\nu)^2$ verses hν and then extrapolating the straight portion of the curve on hν axis at α= 0 as shown in the Fig. 3.6. The band gap energy for the presented samples N1, N2 and N3 is calculated which is much smaller than the bulk Eu^{3+}-SiO_2 composite powder. The extrapolations of the linear portions of the Tauc's plots to $(\alpha h\nu)^{1/2} = 0$ give optical band gaps which are 3.98 eV, 3.90 eV and 3.82 eV respectively for samples N1, N2 and N3.

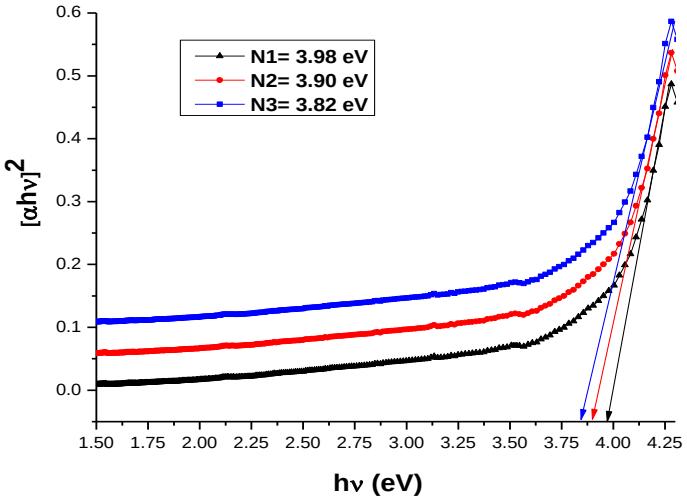

Figure 3.6: Tauc's Plot for samples N1, N2 and N3.

IV. CONCLUSIONS

The XRD analysis proved that monoclinic structure of Eu_2O_3 was well grown along the crystalline phase of silica (quartz). The average size of the nanocrystallites was found to be ~ 30 nm calculated from the diffraction line width based on the D–S formula, W–H plots and TEM histograms. TEM micrographs confirmed the XRD observations regarding the crystallite/particle size of monoclinic phase developed in the nano-dimensional powder. The FTIR peaks of SiO_2 molecule is obtained at 1105, 804 and 476 cm^{-1} in as prepared sample corresponding to asymmetric, symmetric and bending vibrations, respectively. The metal-oxygen bond is appeared at 558 cm^{-1} in the annealed sample which confirms the crystalline phase of prepared nanopowder. In absorption spectra, the band edge was observed at 305 nm along with two small peaks corresponding to the Eu^{3+} 4f-4f transitions. The band gap energy was calculated ~3.90 eV and the observed that with increase in annealing temperature, band gap energy was also slightly decreased. It is concluded that the almost spherical nanoparticles observed in moderately annealed powder are promising materials for potential applications in optoelectronics, biomedical appliances, scintillator, and laser materials and especially for nanophosphors.

ISBN: 978-93-86171-19-1

REFERENCES

[1.] O. M. Ntwaeaborwa, H. C. Swart, R. E. Kroon, P. H. Holloway and J. R. Botha, Surface and Interface Analysis, 38, 458 (2006)

[2.] S. V. Chavan, S. N. Achary, A. K. Tyagi, J. of Alloys and Compounds, 441, 332 (2007)

[3.] J. Mu, L. Liu, S. Kang, Nanoscale Res. Lett., 2, 100 (2007).

[4.] Y. Hu, W. Zhuang, J. Hao, X. Huang, H. He, Open Journal of Inorganic Chemistry, 2, 6 (2012).

[5.] M. Kubus, H. Meyer, L. Kienle, A. M. Klonkowski, J. Non-Crystt. Solids, 355 1333, (2009)

[6.] Y. Ding, H. Min, X. Yu, Mater. Lett., 58, 413 (2004)

[7.] A. Feinle, F. L. Cardinal, J. Akbarzadeh, H. Peterlik, M. Adlung, C. Wickleder and N. Husing, 24, 3674 (2012).

[8.] L. F. Koao, H. C. Swart, R. I. Obed, F. B. Dejena, J. of Lumin., 131, 1249 (2011)

[9.] A. F. Khan, R. Yadav, S. Singh, V. Dutta, S. Chawla, Materials Research Bulletin, 45, 1562 (2010)

[10.] N. A. S. Omar, Y. W. Fen, K. A. Matori, S. H. A. Aziz, Z. N. Alassan, N. F. Samsudin, Procedia Chemistry 19, 21(2016)

[11.] R. Ahlawat, Journal of Alloys and Compounds, 638, 356 (2015)

[12.] S. Duhan, P. Aghamkar, B. Lal, Journal of Alloys and Compounds, 474, 301 (2009)

[13.] Y. K. Kim, H. K. Kim and D. K. Kim, J. Mater. Res., 19, 2 (2004)

[14.] D. Singh, S. Sheoran, S. Bhagwan, S. Kadyan, Cogent Physics, 3, 1262573 (2016)

[15.] T. G. V. M. Rao, A. R. Kumar, K. Neeraja, N. Veeraiah, M. R. Reddy, J. Alloys and Compounds, 557, 209 (2013)

[16.] N. Zhang, R. Yi, L. Zhou, G. Gao, R. Shi, G. Qiu, X. Liu, Mater. Chem. Phys., 114, 160 (2009)

[17.] Rachna, P. Aghamkar, Optical Materials, 36, 337 (2013)